Adsorption, 1, 253–264 (1995)
© 1995 Kluwer Academic Publishers, Boston. Manufactured in The Netherlands.

Interpretation of Water Isotherm Hysteresis for an Activated Charcoal Using Stochastic Pore Networks

R. MANN AND H.N.S. YOUSEF
Department of Chemical Engineering, UMIST, Manchester M60 1QD, England

D.K. FRIDAY
Geo-Centres Inc, Fort Washington, Maryland, U.S.A.

J.J. MAHLE
U.S. Army, CRDEC, Aberdeen Proving Ground, MD 21010, U.S.A.

Abstract. Water vapor adsorption equilibria on activated carbons typically exhibit hysteresis. The size and shape of the hysteresis loop which separates the adsorption and desorption branches is a strong function of the pore size and interconnectivity of the pores. Neither conventional pore filling models nor statistical thermodynamics approaches provide a means for predicting the extent of hysteresis from only adsorption measurements. This work uses the Kelvin Equation in conjunction with the structural concept of a stochastic pore network to describe measured water isotherms on BPL carbon. Using a pore segment distribution function determined from the adsorption branch, it is shown that totally random assemblies underestimate the extent of hysteresis. It is possible, however, to closely fit the measured BPL-water hysteresis loop using a patchy heterogeneity in which a proportion of the larger pores are preferentially located on the exterior, mid-range pores are concentrated in a sub-surface layer and some large pores form shielded voids behind much smaller pores.

Keywords: water isotherms, isotherm hysteresis, activated charcoal, pore size distribution, pore networks

Introduction

Activated carbon is used in countless industrial hygiene and air purification applications. Typically, activated carbon shows a broad range of pore sizes over several orders of magnitude. It is important to understand the nature of water adsorption, since in air with non-zero relative humidity, the presence of water inevitably interferes with the concurrent take-up of any toxic or contaminant compounds in the air.

For adsorbents like activated carbon, it is widely recognised that the extent of sorbate take-up is some combination of surface adsorption and capillary condensation. For water adsorption from humid air, experiments show a pronounced hysteresis between the adsorption and desorption branches of the isotherm (Mahle and Friday, 1989). The hysteresis is suspected to be structurally linked. So far, however, there is no convincing explanation of how the pore space geometry, interior spatial topology and surface texture of an activated carbon can be quantitatively related to adsorption isotherm hysteresis. Grossly simplistic concepts such as the ink bottle explantation (Everett, 1967), are self-evidently inadequate in representing the seemingly intractable complexities of a porous carbon adsorbent simultaneously exhibiting micro-, meso- and macroporosity. Russel and Le Van (1994) have recently presented a summary of traditional pore size distribution characterisation methods, although none of the models reviewed addressed network structures that provide a basis for hysteresis.

The concept of random or stochastic networks of simple pores has been available for some time, following the pioneering work by Fatt (1956). Applications to adsorption using 3-D networks was significantly advanced by Nicholson and Petropoulos (1968). More recently, the crucial impact of pore size distribution on adsorption isotherm hysteresis has been demonstrated by Mann and Thomson (1989), following on earlier work by Mason (1982) and Seaton (1991), showing that pore connectivity and associated percolation theory concepts could influence isotherm hysteresis. Also more recently, Petropoulos et al. (1989) have shown how under partially filled conditions a stochastic network exhibits complex interactions of uptake and permeability. More generally, simple stochastic

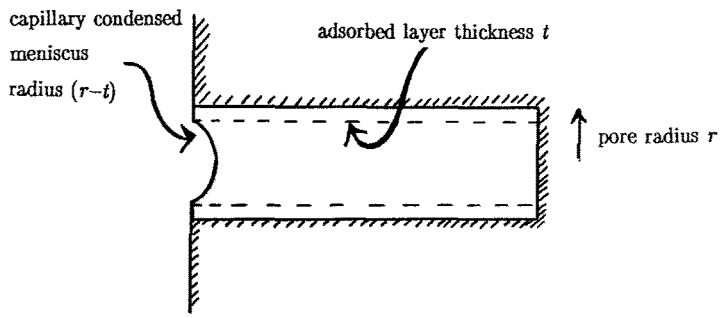

Fig. 1. Simple single pore model.

pore networks have been shown to be capable of explaining a wide variety of phenomena in porous materials, including hysteresis in mercury porosimetry (Androutsopoulos and Mann, 1979; Mann and Golshan, 1981) low recovery in water flood oil displacement (Mann, Androutsopoulos, and Golshan, 1981), catalyst tortuosity under reaction and non-reaction conditions (Sharratt and Mann, 1987), catalyst deactivation by coke laydown (Mann, Sharratt, and Thomson, 1986; Arbabi and Sahimi, 1991) and effective diffusivity in Wicke-Kallenbach experiments (Patwardhan and Mann, 1991).

Stochastic pore networks have been devised as a computationally tractable quantitative treatment of the random interconnected pore spaces encountered in typical porous materials. The latest work on adsorption has included the impact of variation of pore connectivity on isotherm hysteresis (Liu and Seaton, 1994). Rajniak and Yang (1993) have also lately demonstrated how secondary isotherm behavior can be predicted given that the primary adsorption and desorption isotherms are available. In this work, we demonstrate procedures for matching exactly both the adsorption and desorption branches for a specific experimental result for a BPL carbon. It is shown that relatively small structural variations from perfectly random allocation of pores into a network can produce significant variation in the degree of hysteresis observed. Pictorialisations of the deduced networks, albeit only in 2-D and of restricted size amounting to assemblies of pores of the order of thousands, show how the 'texture' of the pore spaces can be visually presented. It is intended ultimately that stochastic pore networks configured by fractal geometry should provide an SEM image reconstruction basis for pore structure evaluation (Mann and Wasilewski, 1990), thereby dispensing with the perpetual necessity to undertake difficult laboratory procedures which in themselves can only provide an indirect measure of the detailed morphology of typically highly complex pore spaces.

Filling and Emptying of a Single Pore

The process of capillary condensation for an 'idealised' cylindrical pore is shown in Fig. 1. The amount of gas adsorbed in such an idealised geometry can be readily calculated from an understanding of the thickness of the adsorbed layer and the Kelvin Equation. The pressure p at which such a pore will fill with condensed gas is given by:

$$r - t = \frac{-2\sigma V_L \cos\theta}{RT \ln\left(\frac{p}{p_{sat}}\right)} \tag{1}$$

In these circumstances as the pressure of the adsorbing gas is raised from zero to p_{sat} and returned back to zero, there will be a small hysteresis between the adsorption and desorption branches of the isotherm caused by the fact that the pore will empty at a lower pressure since the thickness of the adsorbed layer does not affect the meniscus curvature at the pore emptying pressure (Mann and Thomson, 1989). In the event that the thickness t of the adsorbed layer is small relative to the pore radius, any hysteresis between adsorption and desorption will be vanishingly small. For porous materials which show a large hysteresis effect, other mechanisms must be sought to explain the widely different paths exhibited by the adsorption and desorption branches of the isotherm. In this work, for simplicity, any corrections for physical properties in the Kelvin equation, as proposed by Machin and Stuckless (1985), will be left out of the analysis. More complete descriptions of the adsorbed

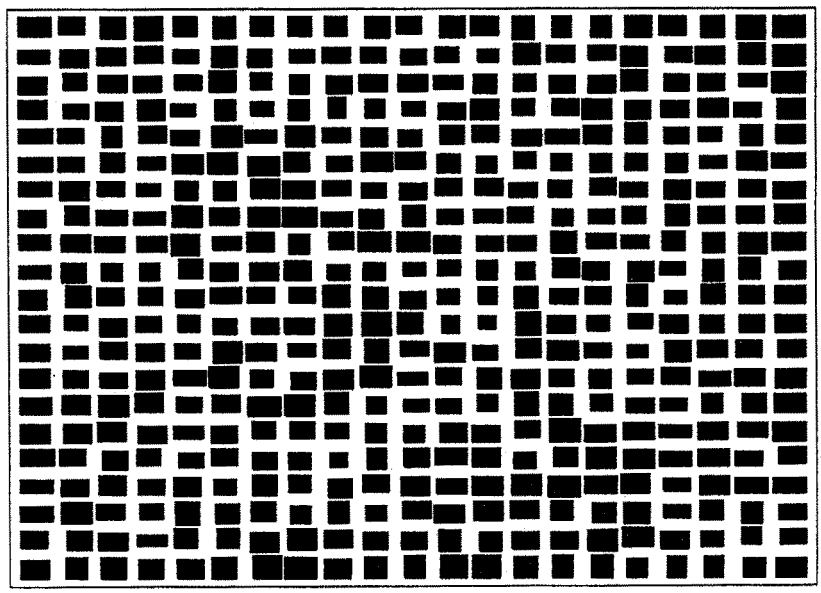

Fig. 2. Pictorialised 20 × 20 network for uniform distribution of pore sizes.

equation of state and the meniscus behavior are as yet unresolved.

Fitting a Network to an Adsorption Isotherm

It is conceptually straight forward to construct networks of any size and to configure them with any stipulated distribution of pore segments. Figure 2 shows a pictorialised example of a 20 × 20 network which comprises uniformly distributed pores between 10 and 4400 Å with a node spacing of 20,000 Å. In Fig. 2, the pores which comprise a uniform distribution have been placed randomly within the network. This means that the size of a given pore is statistically independent of the size of its neighbouring pores. This is termed a stochastic pore network.

The second problem in developing applications of stochastic pore networks is to deduce the statistical distribution of pore segment sizes from a given characterisation method. In this respect, Fig. 3 shows the experimental adsorption/desorption isotherms for a sample of BPL carbon. Fortunately, it is always possible to directly deduce the pore segment distribution for the process of adsorption, since there are no accessibility limitations during capillary filling by condensation. All pores, irrespective of their radius or position in a network, will fill at a relative pressure dictated by the Kelvin Equation (Eq. (1)).

A stochastic network is then constructed from the adsorption branch in Fig. 3 by dividing the cumulative volume ordinate into (say) 10 equal volume increments. The first volume increment from 0 to 0.1 must comprise pores between zero and 156 Å in diameter, since the relative pressure abscissa of 0.48 corresponds to the upper limit of pore size in the incremental volume range. Pore segments are then assumed to be uniformly distributed in this range. The second volume increment (between 0.1 and 0.2) then extends to a relative pressure of 0.54 which must correspond to pores with radii between 156 Å and 185 Å. This argument is applied to each volume increment in turn up to a cumulative volume of 1.0 which obviously corresponds to a complete filling of the network.

The result of this procedure is to provide relative numbers of pores obeying a uniform distribution in each of the ten pore radii ranges. The actual number of pores to be allocated in each of these size ranges is then determined by the size of network to be constructed. The overall numbers of pores have to be coincident with the $2N(N+1)$ pores that form an $N \times N$ stochastic network of pores.

Networks of size 20 × 20 form convenient visualisations in 2-D on a PC screen, thereby enabling an image based assessment of the character of the stochastic network. The 20 × 20 network has 840 pores in total. The fitting to the experimental water isotherm in Fig. 3 by the above procedures gives the result depicted in

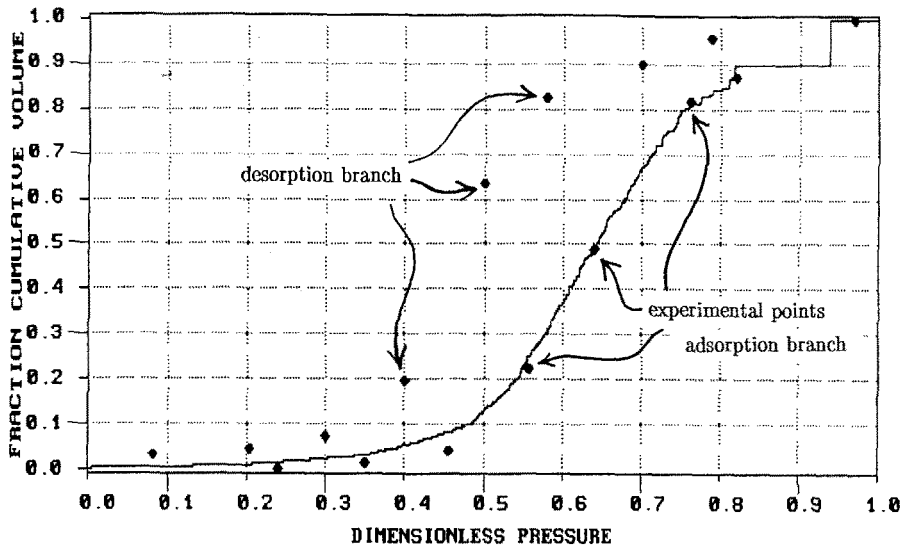

Fig. 3. Experimental adsorption isotherm fitted by a random 20 × 20 network.

224 268 112 383 157 70 113 69 40 160 188 68 198 81 276 78 317 217 167 189
332 125 52 202 235 542 175 233 119 115 101 337 275 228 190 65 198 211 193 158 222
170 34 197 90 158 151 12 46 18 44 99 212 58 254 130 242 232 120 294 308
211 21 25 188 291 164 217 265 14 180 325 21 114 77 267 363 93 83 176 226 252
83 64 120 374 24 34 55 15 65 94 72 36 72 205 351 101 124 305 75 243
173 212 177 305 214 33 4 190 170 238 221 160 59 203 89 32 270 217 262 7 209
15 154 264 213 77 139 161 107 165 62 176 94 78 71 198 272 79 235 445 166
391 115 103 180 260 107 93 383 77 104 74 62 177 122 165 174 78 164 131 251 123
147 177 8 157 212 9 187 232 225 191 12 142 206 144 104 75 237 125 214 73
227 204 287 144 21 191 200 183 290 287 22 113 39 219 242 140 184 46 118 118 114
283 21 52 413 10 194 162 113 161 168 183 314 212 46 2 174 81 133 44 111
187 127 560 107 93 228 64 118 272 172 37 34 272 188 158 28 36 54 50 126 108
192 84 178 189 39 184 225 238 22 187 62 12 148 304 135 113 186 148 46 50
93 113 201 337 123 113 143 36 297 85 175 46 159 31 217 250 313 541 163 116 82
268 311 26 281 237 162 169 159 300 24 235 234 261 210 153 16 85 171 13 195
267 239 247 304 59 188 97 255 158 47 192 69 106 251 195 564 226 150 101 62 9
218 237 123 48 313 85 173 250 479 228 196 16 190 13 118 151 184 211 10 245
13 28 514 300 266 232 11 55 298 7 183 206 166 74 77 8 305 251 201 20 107
291 16 138 81 187 201 37 377 331 266 2 1795 213 88 210 161 205 203 175 17
201 158 175 205 23 189 190 214 172 341 23 33 142 43 231 32 183 155 327 32 196
200 77 31 179 223 146 179 27 218 380 209 237 104 125 214 227 263 22 192 230
327 204 78 10 160 195 274 187 210 66 36 171 202 134 165 37 93 166 184 9 52
178 325 50 69 191 52 327 225 193 275 241 79 96 153 94 91 188 192 154 171
158 284 339 278 114 241 192 285 116 224 203 189 222 146 174 175 218 556 123 24 72
98 196 18 139 89 56 234 103 53 267 274 30 123 125 151 74 150 21 10 8
192 214 199 68 50 161 10 52 258 90 260 163 383 268 105 46 161 79 100 38 138
241 29 26 50 163 49 65 137 151 255 9 227 82 155 186 196 232 59 71 183
81 126 165 267 209 46 29 39 20 85 130 136 203 169 66 228 46 132 33 390 146
350 56 193 7 297 209 89 163 187 85 170 139 178 311 350 32 139 182 136 130
208 130 119 220 260 141 3 45 169 218 130 165 189 163 214 177 110 37 244 321 50
139 196 17 112 165 82 195 137 314 120 184 31 176 126 258 153 186 444 360 221
128 181 192 323 249 174 223 237 141 291 155 192 39 100 158 340 93 215 109 400 7
213 363 257 51 41 136 306 41 212 247 2 69 152 67 252 159 6 440 87 26
18 40 180 188 295 380 124 180 82 164 50 61 263 2 240 75 147 59 206 71 231
187 205 208 215 101 259 33 105 129 181 238 25 155 145 237 59 209 14 24 115
172 148 196 104 18 211 180 124 46 186 93 92 255 470 21 121 258 66 159 181 98
37 187 147 36 199 242 112 251 115 225 134 208 351 353 388 180 27 287 5 136
295 159 54 111 130 79 179 197 211 254 214 128 203 230 165 231 173 243 9 122 84
228 159 170 83 85 150 236 132 44 153 190 112 90 114 125 159 182 121 92 238
223 126 3 104 351 134 3 227 28 199 157 206 123 122 114 190 84 206 95 127 254
161 139 18 330 179 170 58 295 173 16 67 28 216 214 146 132 110 51 160 19

Fig. 4. Numerical values of 840 pores in fitted random network (20 × 20).

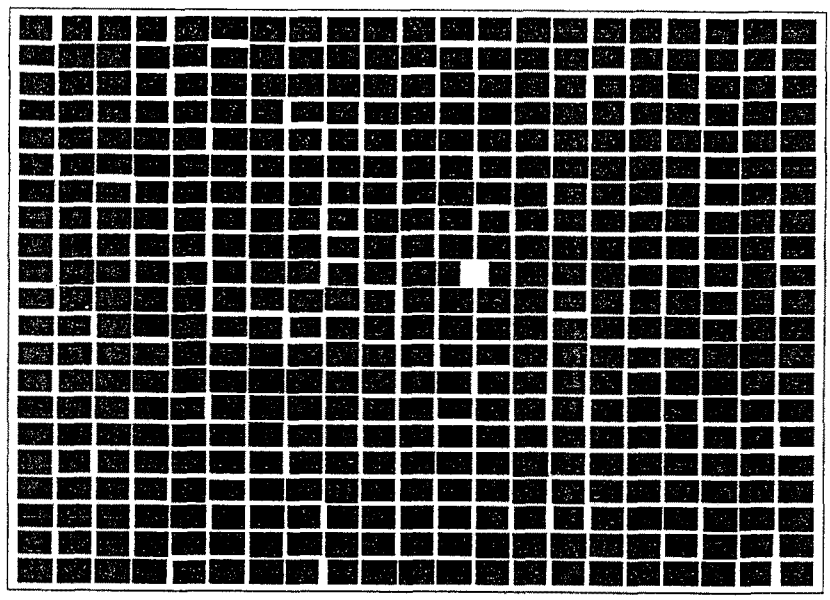

Fig. 5. Pictorialisation of the fitted random network.

Fig. 4 which show the 840 pore sizes individually as placed randomly in the network. Figure 5 then shows a pictorialisation of the network of Fig. 4. The corresponding number distribution and volume distribution histograms are presented in Figs. 6(a) and 6(b) respectively. The juxtaposition of the two figures is striking, since it is immediately evident that the majority of the pore volume is contained in just a few large pores. In fact of the total 840 pores, the five largest pores have radii of 1795, 564, 560, 556, and 542, which account for some 14% of the total network volume. In contrast, 92% by number of the pores have sizes less than 300 Å. It is not immediately obvious, but the accessibility of the few large pores is controlled by the preponderance of much smaller pores. It is inevitable that a large proportion of the larger pores will be hidden amongst smaller ones and this could be expected to lead to a pronounced hysteresis effect.

Predicting the Desorption Branch of the Isotherm

Once the network in Fig. 4 has been completely filled by condensate, the emptying process, on reduction of the water pressure, will initiate from the largest pore on the exterior. This is of size 391 Å located at row 8 and column 1. No further emptying occurs because the neighbor pores are of sizes 147, 115 and 15 Å. This single emptying step takes place at a relative pressure of 0.75. The desorption process is followed step by step. A significant hysteresis loop is generated because the largest proportion of the larger pores are shielded amongst smaller pores. The full desorption (or emptying) branch is presented in Fig. 7 for the detailed calculations of the entire 840 pores.

As can be seen from Fig. 7, the non-emptying of large hidden pores initially causes the predicted desorption to lie above the experimental result for random placement of pores. However, at around a relative pressure of 0.55, corresponding to the emptying of pores of radius 189 Å, there occurs a very large emptying of a set of connected pores which causes the desorption branch to fall suddenly below the experimental result. In qualitative terms, this behavior is linked to the percolation threshold of those pores lying below the size of 189 Å. The result is that some 70% of the whole network dimensionless volume empties as the relative pressure falls from 0.55 to 0.44. Below this percolation type threshold, there is almost negligible shielding possibility of large pores behind small ones. As a result the desorption branch becomes closely coincident with the adsorption one, so that they are effectively indistinguishable.

If these simulations are now carried out for a network of double the size, i.e., a 40 × 40 network comprised

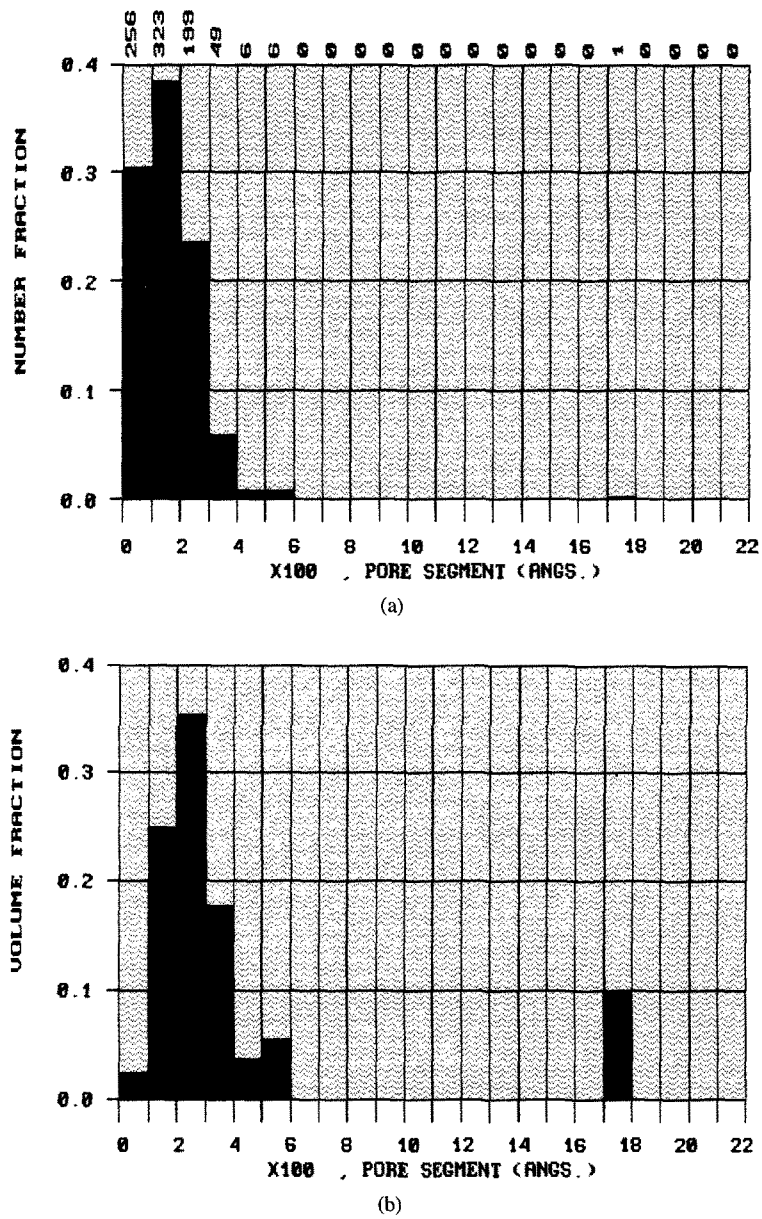

Fig. 6. (a) Number distribution of pore segments. (b) Volume distribution of pore segments.

of 3280 pores, there is little visually detectable change in the adsorption branch of the isotherm. However, because of the increased potential for shielding of large pores behind smaller ones, the desorption branch is always significantly displaced above that for the smaller 20×20 network. As a result, although the hysteresis loop is enlarged, the quality of fit to the experimental result is effectively made worse, especially in the relative pressure range from 0.55 down to 0.44.

Effect of Structure Re-ordering on the Desorption Branch

So far, the two networks examined have been entirely randomised, so that the size of a pore at any position is taken to be independent of the size of any neighboring pores. If some order is to be introduced into the assembly of pores in forming a network, it is first of all quite clear that, irrespective of the nature of re-structuring,

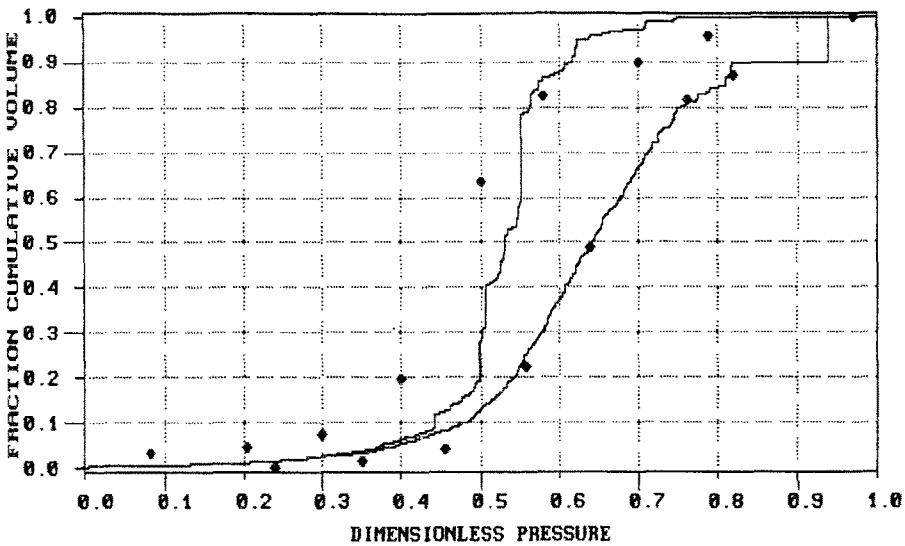

Fig. 7. Predicted desorption isotherm for random network (20 × 20).

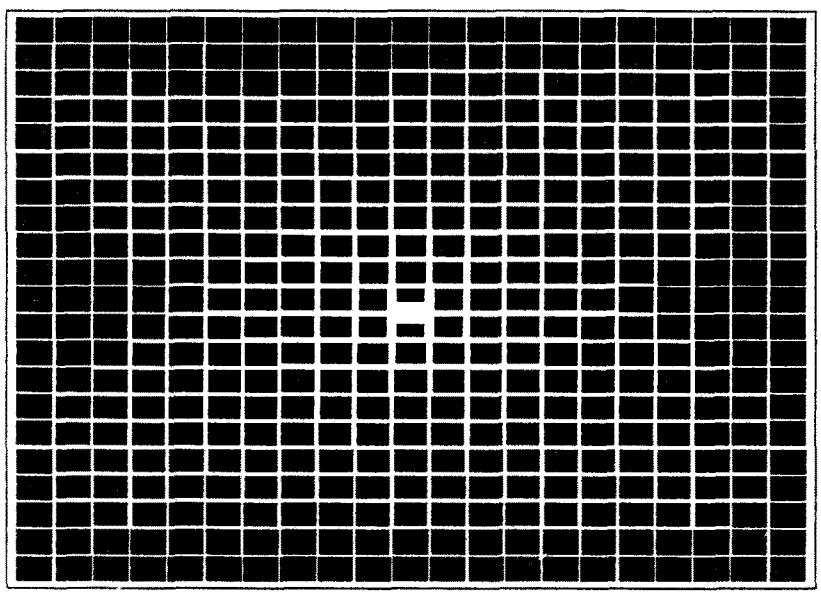

Fig. 8. Spirally wound networks of pores: largest pores on interior/smallest pores on exterior.

the adsorption (or filling) branch will be entirely unaffected. It is however evident that the effects of restructuring from a random basis will show up in the desorption isotherm.

This can be easily demonstrated with respect to an illustrative extreme of re-ordering whereby the full set of random pores are assembled in rank order and then spirally 'wound' into position in the network. If the spiral rewinding places the largest pore at the centre and the smallest pore at the exterior, the pictorialised 20 × 20 network of Fig. 4 appears as shown in Fig. 8. This network, which has pore sizes graded in size from the outside to the centre will not empty of sorbate until the value of p/p_{sat} corresponds to a very small pore of ra-

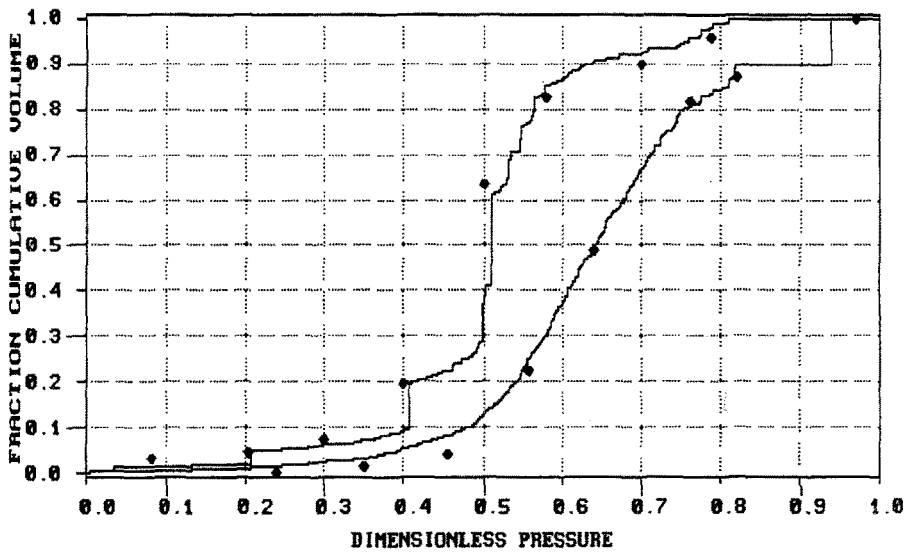

Fig. 9. Isotherms predicted using patchy heterogeneity.

dius 29 Å. This represents the largest possible hysteresis. In contrast, the counterpart spirally wound network with the smallest pore at the centre and the largest on the exterior gives zero hysteresis, so that the desorption branch is then exactly coincident everywhere with the adsorption.

It is therefore clear that a huge variation of possibilities for the desorption branch exists according to extents of restructuring which lie between complete randomness and the extreme of spiralling size ranked assembly.

Figure 9 then shows an example of a close match of the experimental desorption branch which has been achieved by a small extent of structural recordering. This reordering has three conceptual components. These can be briefly summarised as (i) a preferred location of some of the largest pores on the exterior surface, (ii) a sub-surface layer comprised of a lower proportion of mid-size range pores and (iii) a small proportion of shielded voids in which some of the largest pores are isolated amongst some of the smallest ones. The structural reordering, which we term a patchy heterogeneity, leaves 95% of the pore network completely random, and requires the adjustment of only some 54 pores out of the total of 840 for a 20 × 20 network.

The full details of the structural re-ordering are presented in Fig. 10 in two parts. Figure 10(a) shows the original locations of the 54 manipulated pores. The remainder of the pores in the network which are not affected are shown as asterisks. The size of these unaffected pores can be read from Fig. 4. Figure 10(b) then indicates the nature of the changes made and shows the adjusted pores in their new positions. The three stages of adjustments are then as follows.

Firstly, in order to provide for an increased extent of desorption over the relative pressure range from 1.0 down to 0.7, the small number of pores sized from 541 Å down to 400 Å have been relocated on the network exterior. These 8 pores are indicated by enclosure in a single box in Fig. 10(b). The largest of these pores gives an initial desorption at a relative pressure of 0.81 with the remaining pores emptying down to a relative pressure of 0.75. This improves the initial fit of the isotherm (see Fig. 7 for comparison with the fully random network) which is indicative of an increased probability for larger pores to be located at the network exterior.

Secondly, the subsequent accelerated rate of emptying observed for the random network is avoided by replacing some of the exterior pores of size 390 Å down to 295 Å to more interior positions. These are shown underscored in Fig. 10(b) and amount to just 11 pores. These pores have been switched with 11 pores in the range 165 Å down to 158 Å which have been replaced into the vacated 11 pore exterior positions. These pores which have been moved outward are shown as overscored in Fig. 10(b). This second phase of adjustment amounts to a tendency for the immediately inner layers

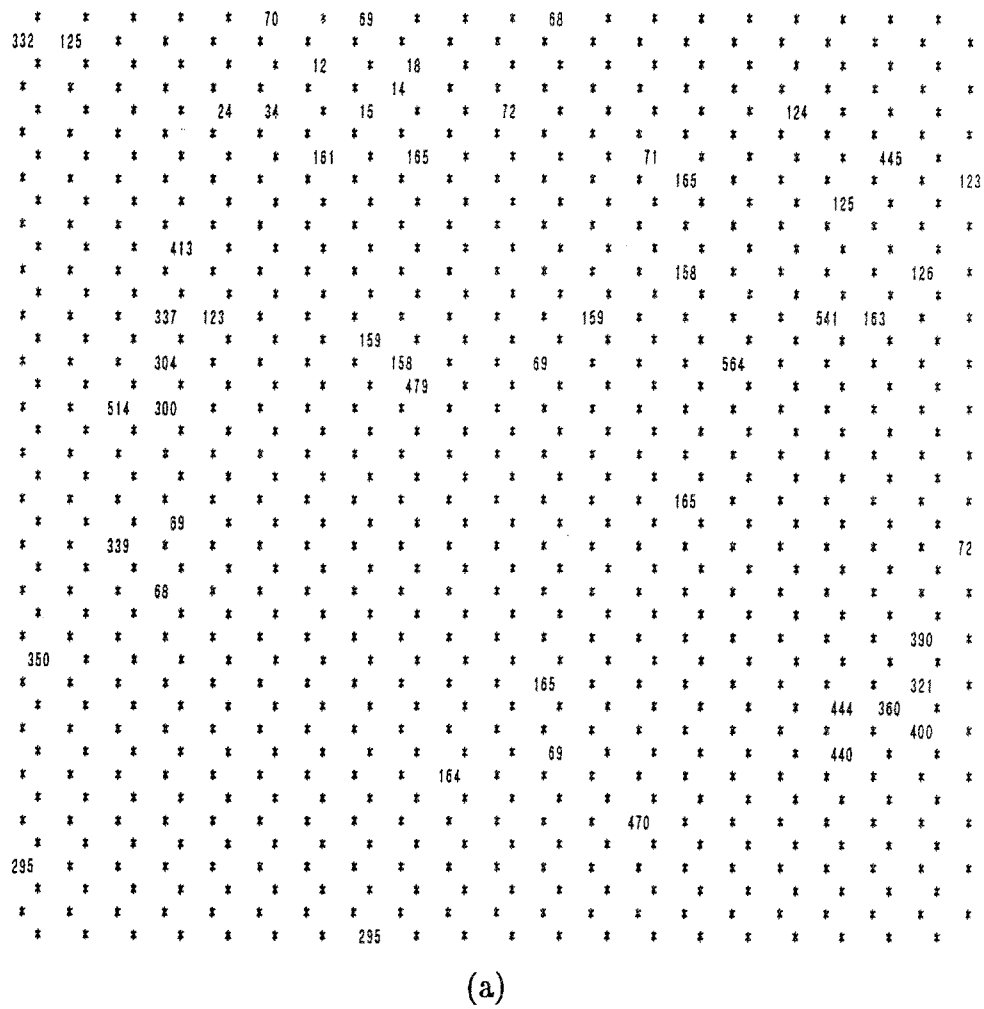

Fig. 10. Details of local re-ordering with patchy heterogeneity. (a) Pores subjected to repositioning; (b) pores as repositioned.

of pores to be smaller on average than for the whole network. As a result of this adjustment, a steadily progressive desorption is maintained from a relative pressure of 0.75 down to 0.5.

The third and final phase of heterogeneity involves the requirement to avoid a sudden onset of emptying related to a percolation threshold in the relative pressure range from around 0.5, so that there is still a significant water retention at a relative pressure as low as 0.4. This can be achieved by restricting the emptying of the five largest pores by surrounding them by smaller ones. Just three such "shielded voids" are necessary to achieve this and these are shown in large "boxed" conglomerates of pores in Fig. 10(b). The first to empty would be the largest 1795 Å pore surrounded by pores sized from 126 Å to 123 Å. The second conglomerate of 3 large pores forming a single void empties between 72 Å and 68 Å. The final shielded void with a pore size of 524 Å is shielded by very small pores of size 34 Å to 12 Å which empties at a relative pressure of 0.036. As a result of the creation of these three shielded voids, the final portion of the desorption emptying now closely follows the experimental result.

Finally, for the deduced structure at a 20 × 20 size, Fig. 11 shows the desorption sequence when 1/4, 1/2 and 3/4 of the adsorbed water has been removed by desorption (number basis). It can be seen that the largest pore size 1795 Å is still filled with water at 1/2 removal, but empty when 3/4 of the desorption has taken place.

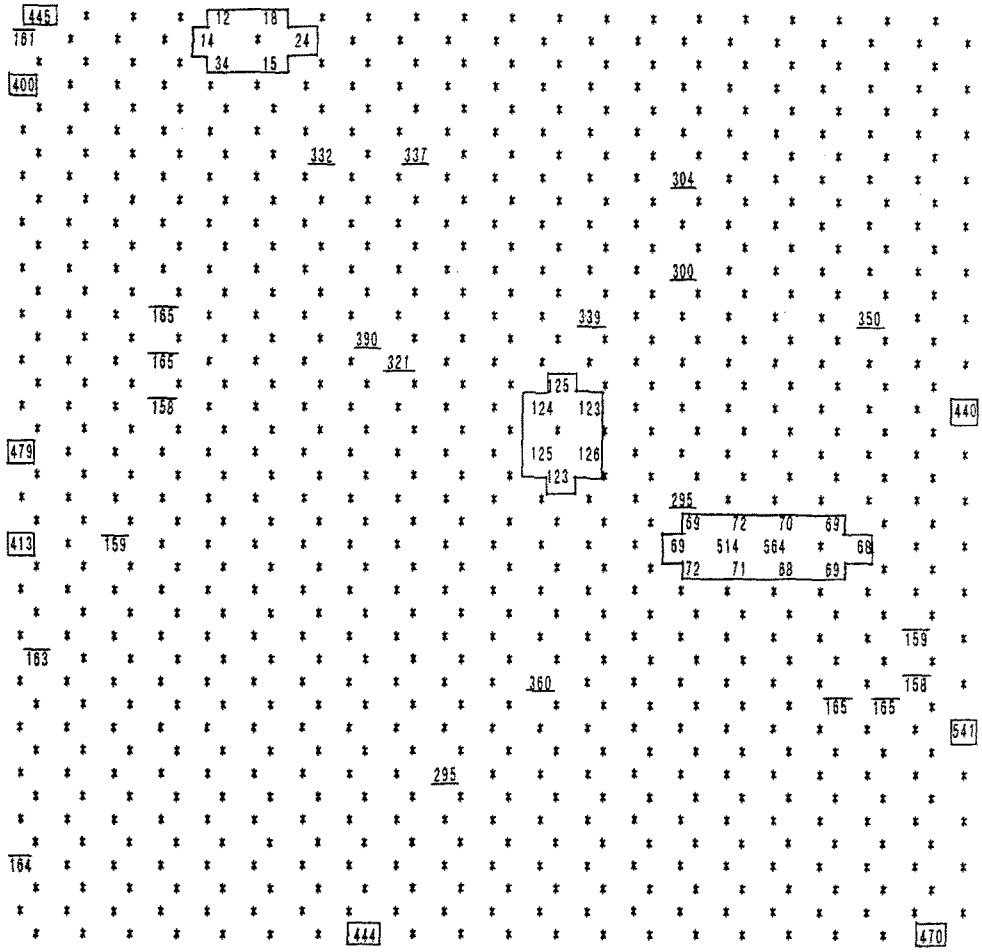

(b)

Fig. 10. (Continued.)

Discussion

Although the particular quantitative details of this restructuring should not be taken to possess precise significance, the concept of partial restructuring comprising a patchy heterogeneity, as distinct from exact randomness, may well be the appropriate qualitative concept to explain the desorption isotherm which has been experimentally measured. It is then possible that this concept of patchy heterogeneity is related to the processing procedures which have resulted in the formation of the activated carbon particles. In any event, it is clear that partially ordered/partially random structures have the capability to explain and describe the water isotherm hysteresis encountered in this case.

Finally, it is important to recognise that the validity of these detailed results of structural re-ordering from perfect randomness are model dependent. Both topology and connectivity as well as individual pore shape geometry will vary the shape and intensity of any hystereous loop. Therefore the deduced psd for the regular 2-D 6-connectivity square network used here is obviously not wholly unique. Furthermore, it is likely that such a deduced psd will also be influenced by improved understanding of the thermodynamics of the pore surface/adsorbate interactions, so that further work in this area will assist the development of more valid psd characterisation.

Ultimately, of course, this approach needs to be deployed and tested with 3-D pore network models.

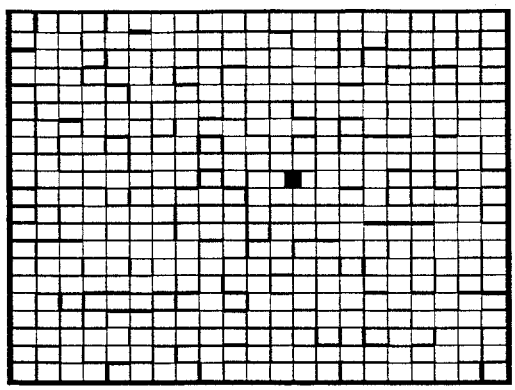

network filled with sorbate water

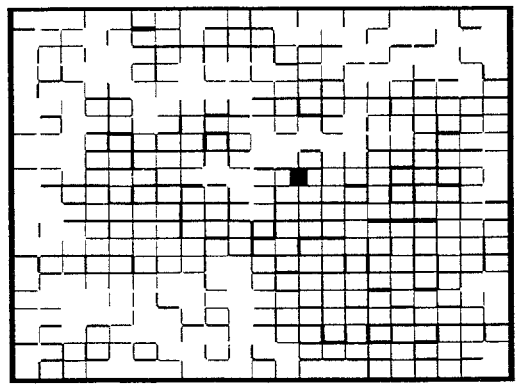

one–quarter desorbed

one–half desorbed

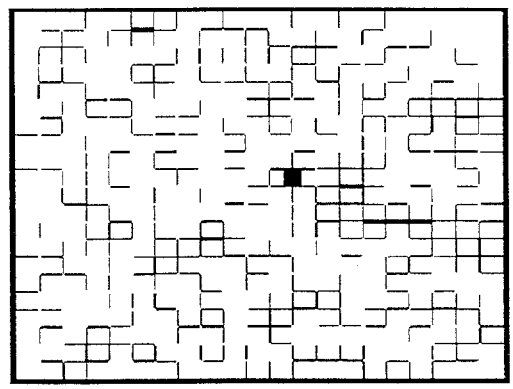

three–quarters desorbed

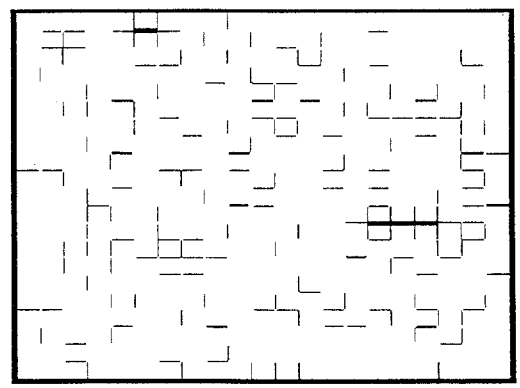

Fig. 11. Pictorialised desorption sequence for fitted network.

Conclusions

1. The concept of a simple 2-D stochastic pore network of cylindrical pore segments can be readily applied to deduce the intrinsic pore segment distribution for a specific sample of a BPL activated charcoal. The deduction of the pores size distribution (psd) is simpler than for mercury porosimetry since in adsorption by capillary condensation, there are no accessibility limitations.
2. The extent of hysteresis between adsorption and desorption has been shown to be attributable to the way pore segments are assembled together.
3. The most extreme hysteresis between the adsorption and desorption branches occurs when the pore sizes are spirally allocated into a network with the largest pores on the interior sequenced to the smallest pores on the exterior of the network. There is a negligible hysteresis for the reversed spiral assembly which has the largest pores on the outside of the network and the smallest ones at the centre.
4. For the BPL sample studied, random assembly of pores produced only a poor approximation of the experimental hysteresis loop.
5. An exact replication could be achieved by using a simple patchy heterogeneity which required manipulation of only 5% of the pores forming the random network. This partial restructuring involved larger pores preferentially on the exterior, an inner layer with a smaller proportion of mid-size pores and a small number of shielded large voids.

Nomenclature

p	vapor phase partial pressure of sorbate
p_{sat}	saturation vapor pressure of sorbate
R	gas constant
r	pore radius
T	absolute temperature
t	adsorbed layer thickness
V_L	molar volume of adsorbed phase
σ	surface tension
θ	contact angle

References

Androutsopoulos, G.P. and R. Mann, "Evaluation of Mercury Porosimeter Experiments Using a Network Pore Structure Model," *Chem. Eng. Sci.*, **34**, 1203–1212 (1979).

Arbabi, S. and M. Sahimi, "Computer Simulations of Catalyst Deactivation—II. The Effect of Morphological, Transport and Kinetic Parameters on the Performance of the Catalyst," *Chem. Eng. Sci.*, **46**, 1749–1755 (1991).

Everett, D.H., "Adsorption Hysteresis," in *The Solid Gas Interface* (E. Alison Flood, Ed.), 1055, Marcel Dekker, New York, 1967.

Fatt, I., "The Network Model of Porous Media I: Capillary Pressure Characteristics," *Petrol. Trans. A.I.M.E.*, **207**, 144 (1956).

Liu, H. and N.A. Seaton, "Determination of the Connectivity of Porous Solids from Nitrogen Sorption Measurements—III Solids Containing Large Mesopores" *Chem. Eng. Sci.*, **49**, 1869–1878 (1994).

Machin, W. and J.T. Stuckless, "Capillary-Condensed Water in Silica Gel," *J. Chem. Soc. Faraday Trans.*, **81**, 597 (1985).

Mahle, J.J. and D.K. Friday, "Water Adsorption Equilibria on Microporous Carbons Correlated Using a Modification to the Sircar Isotherm," *Carbon*, **27**, 835–843 (1989).

Mann, R., G.P. Androutsopoulos, and H. Golshan,"Application of a Stochastic Network Pore Model to Oil Bearing Rock with Observations Relevant to Oil Recovery," *Chem. Eng. Sci.*, **36**, 337–346 (1981).

Mann, R. and H. Golshan, "Application of a Stochastic Network Pore Model to a Catalyst Pellet," *Chem. Eng. Comm.*, **12**, 377–391 (1981).

Mann, R., P.N. Sharratt, and G. Thomson, "Deactivation of a Supported Zeolitic Catalyst: Diffusion, Reaction and Coke Deposition in Stochastic Pore Networks," *Chem. Eng. Sci.*, **41**, 711–718 (1986).

Mann, R. and G. Thomson, "Interpretation of Low Temperature Gas Adsorption and Desorption Using Stochastic Pore Networks," in *Adsorption: Science & Technology*, Al.E. Rodrigues et al. (Eds.), pp. 63–77, Kluwer Academic Publishers, 1989.

Mann, R. and M.C. Wasilewski, "Towards a Fractal Computer Graphic Basis for Characterisation of Catalyst Pore Structure by Image Reconstruction," *Trans. I. Chem. E.*, **68** Part A, 177–184 (1990).

Mason, G., "The Effect of Pore Space Connectivity on the Hysteresis of Capillary Condensation in Adsorption-Desorption Isotherms," *J. Coll. Int. Sci.*, **88**(1), 36 (1982).

Nicholson, D. and J.H. Petropoulos, "Capillary Models for Porous Media II: Sorption-desorption Hysteresis in 3-D Networks," *Brit. J. Appl. Phys. (J. Phys. D)*, **1**, 1379 (1968).

Patwardhan, A.V. and R. Mann, "Effective Diffusivity and Tortuosity in Wicke-Kallenbach Experiments: Direct Interpretation Using Stochastic Pore Networks," *Trans. I. Chem. E.*, **69**, Part A, 205–207 (1991).

Petropoulos, J.H., J.K. Petrou, and N.K. Kanellopoulos, "Explicit Relation Between Relative Permeability and Structural Parameters in Stochastic Pore Networks," *Chem. Eng. Sci.*, **44**, 2967–2978 (1989).

Rajniak, P. and R.T. Yang, "A Simple Model and Experiments for Adsorption-Desorption Hysteresis: Water Vapour on Silica Gel," *A.I.Ch.E. Jl.*, **39**, 774–781 (1993).

Russell, B.P. and M.D. LeVan, "Pore Size Distribution of BPL Activated Carbon Determined By Different Methods," *Carbon*, **32**(5), 845 (1994).

Seaton, N.A., "Determination of The Connectivity of Porous Solids From Nitrogen Sorption Measurements," *Chem. Eng. Sci.*, **46**(8), 1895 (1991).

Sharratt, P.N. and R. Mann, "Some Observations on the Variation of Tortuosity with Thiele Modulus and Pore Size Distribution," *Chem. Eng. Sci.*, **42**, 1565–1576 (1987).